

# PHYSICAL REVIEW D

## PARTICLES AND FIELDS

THIRD SERIES, VOL. 8, No. 5

1 September 1973

### Measurements of the Polarization Parameter in $\pi^\pm p$ Elastic Scattering Between 2.50 and 5.15 GeV/c $\dagger\dagger$

J. A. Scheid,\* N. E. Booth,\* G. Conforto,<sup>§</sup> R. J. Esterling,<sup>§</sup> J. H. Parry,<sup>||</sup> and D. J. Sherden\*\*  
*The Enrico Fermi Institute and Department of Physics, The University of Chicago, Chicago, Illinois 60637*

A. Yokosawa

*Argonne National Laboratory, Argonne, Illinois 60439*

(Received 26 December 1972)

The polarization parameter in  $\pi^\pm p$  elastic scattering has been measured at several momenta in the range 2.50-5.15 GeV/c pion laboratory momentum and covering the range in  $t$  approximately from  $-0.2$  to  $-2.0(\text{GeV}/c)^2$ . The data show positive polarization for  $\pi^+p$  scattering, having a dip near  $t = -0.6 (\text{GeV}/c)^2$  and becoming relatively large at greater values of  $-t$ . The results for  $\pi^+$  and  $\pi^-$  scattering are approximately equal in magnitude but of opposite sign. The data have been analyzed to separate the components, which are symmetric and antisymmetric with respect to pion charge, and to show both the  $t$  and  $s$  dependence of each part.

#### I. INTRODUCTION

We report here the results of the measurements of the polarization in  $\pi^\pm p$  elastic scattering at several pion laboratory momenta in the range from 2.50 to 5.15 GeV/c and in the four-momentum-transfer-squared range from  $-0.2$  to  $-2.0 (\text{GeV}/c)^2$ . The  $\pi^\pm p$  data were taken at beam momenta of 2.50, 2.75, 2.93, 3.25, 3.75, 4.40, and 5.15 GeV/c. These measurements were made at the Argonne National Laboratory Zero-Gradient Synchrotron (ZGS), using the Argonne polarized proton target as part of an experiment in which the polarization in forward  $pp$ , forward  $K^+p$ , and backward  $\pi^+p$  elastic scattering were also measured.<sup>1-4</sup>

In the region below 2.5 GeV/c extensive measurements of polarization have been made.<sup>5-7</sup> The high-energy forward region has been investigated<sup>8</sup> in experiments at 6, 8, 10, and 12 GeV/c, and more recently<sup>9,10</sup> at 6, 10, 14, and 17.5 GeV/c. Recently results for  $\pi^\pm p$  polarizations up to 2.74 GeV/c have appeared.<sup>11-13</sup>

Polarization data taken in the intermediate re-

gion serve a threefold purpose. At low energies, where the total cross sections show considerable structure,<sup>14</sup> they contribute to the determination of the partial-wave amplitudes and therefore of the spin and parity of the direct-channel resonances.<sup>6,7</sup> At higher energies the data have been interpreted with some success using models based on the dominance of meson exchanges in the crossed channel,<sup>15,16</sup> and measurements in the intermediate energy region test the extrapolation of these models to lower energies. Finally, data at intermediate energies connecting the regions in which the direct and crossed channels dominate, provide a test for models joining the high- and low-energy regions through sum rules and duality.<sup>16</sup> The data presented here bridge the gap between these two domains in regular momentum intervals and, of particular importance, extend polarization measurements to a greater range in  $t$ .

#### II. EXPERIMENTAL PROCEDURE

The following is a brief description of the experimental apparatus and procedure with special attention to the forward  $\pi p$  data. A more detailed

description of the experiment is presented in Refs. 2 and 17. The general method is the measurement of the asymmetry in the differential cross section produced by reversing the target polarization. The scattering was done in the vertical plane with the target polarized in the directions perpendicular to the scattering plane.<sup>18</sup> Target polarization was measured using nuclear magnetic resonance and the recoil proton polarization computed as the ratio of the asymmetry to the target polarization.

The extracted ZGS beam was focused on a copper target to produce a secondary beam, taken at  $0^\circ$ , with a momentum acceptance of  $\pm 3.5\%$ . Beam compositions varied between 50% pions at 2.5 GeV/c and 25% pions at 5.15 GeV/c for positives, while the negative beam was essentially all pions. The beam transport system delivered  $10^6$  particles per pulse to the polarized proton target.

The target was lanthanum magnesium nitrate (LMN) doped with 1.5% neodymium and containing 3% free protons in the water of hydration. Target polarization was monitored automatically at frequent intervals during the runs and was typically 0.55 with an error of  $\pm 10\%$ .

A simplified schematic of the apparatus is shown in Fig. 1. Electrons in the beam were eliminated with a gas threshold Čerenkov counter and a second similar counter provided the pion signal. The beam was horizontally dispersed in momentum at an intermediate focus where a scintillation-counter hodoscope divided the beam into seven momentum bins of  $\pm 0.5\%$  resolution. Before reaching the target, beam particles passed through two square arrays of scintillation counters defining the divergence and position of each particle as it entered

the target.

Scattered particles were detected in hodoscopes consisting of two layers of scintillators, the first layer defining the polar angle ( $\theta$ ) of the scattered particles, and the second layer their azimuthal angle ( $\phi$ ). Solid angle about the target not subtended by these hodoscopes was covered by various veto counters. For the forward pion data the kinematics and the geometry of the target were such that all good events consisted of a pion in the upper arrays (A1 and A2) accompanied by a recoil proton in the lower array (B). Pions were taken to define the scattering angle and the angular distributions of the conjugate protons were collected for each defining angle.

A valid beam particle was defined as a coincidence between a beam timing counter and one counter in each of the five beam hodoscopes. An event trigger was produced by a coincidence between a valid beam particle, a signal from the B array, and a signal from either the A1 or A2 array.

After passing through discriminators, all counter signals were stored temporarily in 100-nsec cables while the fast-logic circuitry tested the validity of the event. A good event was gated by the fast logic into an array of bistable circuits, one for each of the counters in the apparatus. The state of these was then read into an on-line EMR 6020 computer for analysis and storage.

In the computer, events for which more than one particle were detected in any counter array or for which the  $\theta$  and  $\phi$  hodoscopes did not correspond to the same array were rejected. Valid events were encoded and written on magnetic tape. When not receiving and encoding data, the comput-

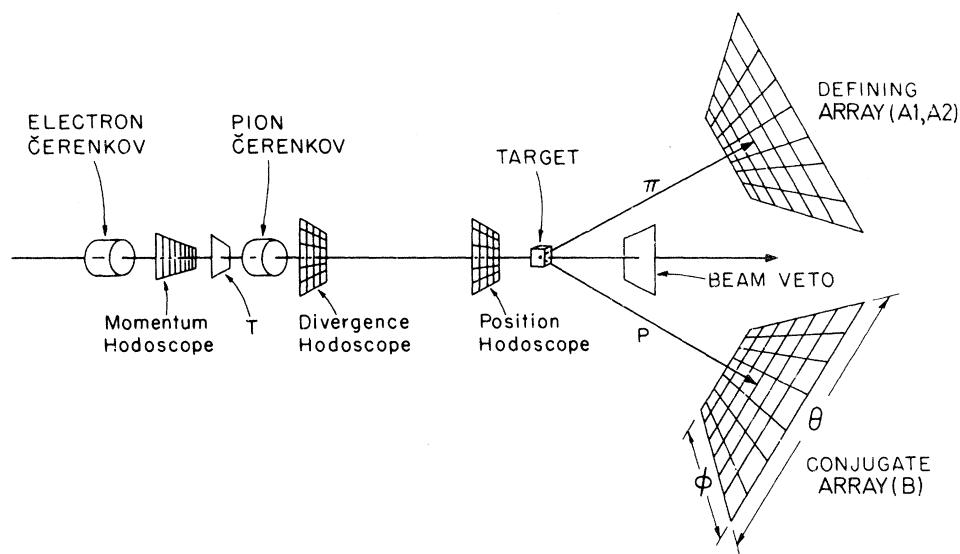


FIG. 1. Schematic view of the arrangement of counters in the beam and about the target.

er performed calculations using information furnished by the beam hodoscopes on the momentum of the beam particle, its angle of incidence, and the vertical and horizontal position of the interaction point in the target. In this calculation the scattering angles were shifted to correspond to an event for which the incident beam particle was on the central ray of the beam, the scattering was in the vertical plane exactly, and the final-state particles lost no energy in the material of the target.

For each defining angle, distributions of the conjugate protons were then formed from the shifted events centered on the kinematically determined point for the proton in the  $B$  hodoscope. The position and spread of these distributions included the effects of the momentum spread of the beam, the finite size of the beam and counters, the finite size of the target, the magnetic field of the target, and the multiple scattering and energy loss in the target. These factors were considered in a preliminary Monte Carlo simulation of the scattering used to calculate the position and width to be expected in the conjugate distributions.

Conjugate events were collected in three distributions: a  $\phi$  distribution, consisting of the events in each conjugate  $\phi$  bin for all conjugate  $\theta$  bins; a coplanar  $\theta$  distribution, containing events in each conjugate  $\theta$  bin for all central  $\phi$  bins; and a non-coplanar  $\theta$  distribution, containing conjugate events for all  $\phi$  bins on either side of the central region of the  $\phi$  distribution. Events due to elastic scattering from free protons were expected in the central region superimposed on a background due to inelastic processes and quasielastic scattering on bound nucleons in the complex nuclei of the target. The Fermi energy of bound nucleons causes a broadening of the quasielastic peak, making it possible to distinguish these events from those due to elastic scattering from free, polarizable protons. The separation of the free peak from the background was thus accomplished by requiring coplanarity in the  $\phi$  direction and by elastic scattering kinematics in the  $\theta$  direction.

The data analysis began with the Monte Carlo program which produced initial information on the position and width to be expected in the distributions, and the coefficients used to shift the events into the canonical form. Using this as input, the data were collected and processed by the on-line program. After examining the distributions produced by the on-line program, the cuts defining the central regions were generally revised and the data were analyzed again by an off-line version of the same program.

With the distributions in final form, a check on the consistency of the data was made by a program

which compared counters in all runs for a particular momentum and particle. Any atypical counters or runs became evident and were corrected or eliminated.

Two methods of background subtraction were then used, generally giving results in good agreement. Preliminary results were obtained using backgrounds calculated from the noncoplanar distributions by normalizing the noncoplanar events to those sections of the coplanar distribution outside the free proton peak. In the second method, background was computed from the coplanar  $\theta$  distribution alone by fitting the counts outside the free peak to a polynomial of five terms or less. This was extrapolated to the region under the elastic peak and subtracted as background. The final results presented here were obtained by this method.

### III. RESULTS

The data are presented in Fig. 2 and in Tables I and II. Table III contains the results obtained for  $\pi^+p$  at backward angles which have been discussed in a previous publication.<sup>3</sup> At 4.40 GeV/c [see Fig. 2(f)] the analysis was extended to smaller angles by a more elaborate method than discussed in Sec. II. Low-energy protons, conjugate to very forward pions, produced broad peaks due to greater multiple scattering and spread in energy loss in the target. Using information from the position hodoscope immediately before the target, these events were separated into five distributions corresponding to different thicknesses of target material traversed by the recoil proton after the collision. Owing to the breadth of these distributions, the background fitting was less well determined and an additional error was calculated from the difference between the two curves representing the extremes of a reasonable fit to the background.

Special care was taken to avoid possible artificial asymmetries. Runs were taken in matched pairs of opposite target polarization with nearly the same number of incident particles and were essentially identical in other respects. Two major sources of systematic error in an experiment of this kind are the measurement of target polarization and the possibility of asymmetry in beam normalization. A careful study was done of the target polarization data by dividing the runs into several smaller groups for each momentum and comparing average polarizations of the subgroups. This provided a check on the target polarizations, and correction factors were applied to the target polarizations making the subgroup averages consistent.

The largest error in beam normalization arose from targeting efficiency because the beam spot size was larger than the size of the target. Es-

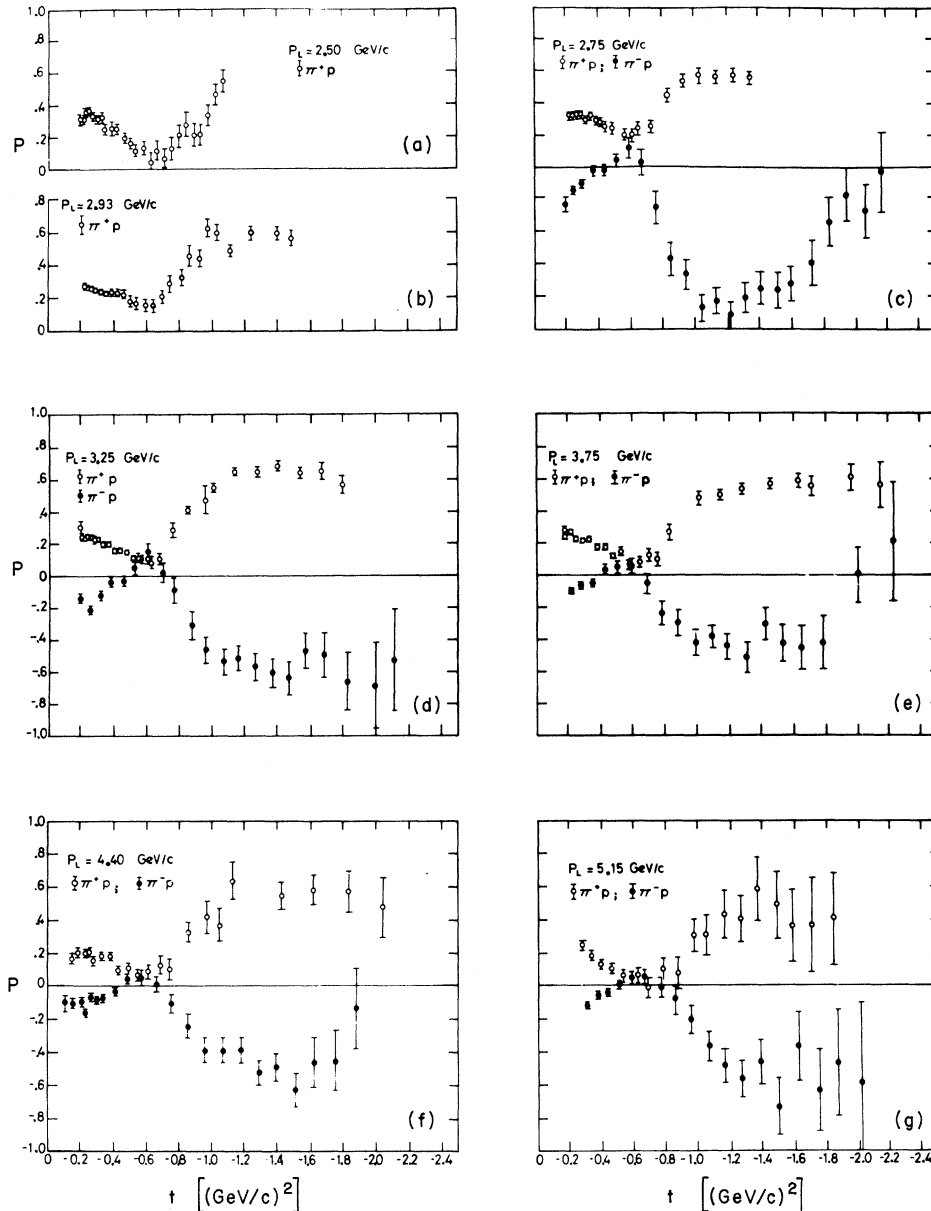


FIG. 2. Measured polarization in forward  $\pi^+p$  and  $\pi^-p$  elastic scattering at 2.50, 2.75, 2.93, 3.25, 3.75, 4.40, and 5.15 GeV/c pion laboratory momentum.

timates of the errors in beam normalization were obtained from the consistency checking program by comparing the sizes of the unpolarized background outside the elastic region. Run to run normalizations were found to agree to within 2%. When all runs of a given momentum and sign of target polarization were combined, the backgrounds for the two signs of target polarization were found to agree within 1% for all momenta. The results of the consistency checking program indicated that the apparent asymmetry in back-

ground was constant throughout the entire angular region, thus giving us confidence that it was simply due to beam normalization rather than to real asymmetries in the background. Consequently, and in view of the smallness of the correction, the results of the consistency checking program were used to adjust the beam normalization of each run to make the unpolarized backgrounds agree with the average of all runs. We thus feel confident that the beam normalizations are good to 0.5%. The effect of this uncertainty depends upon the

TABLE I. Measured values of polarization in  $\pi^+p$  elastic scattering.

Beam laboratory momentum (GeV/c)	$t$ [(GeV/c) <sup>2</sup> ]	$P$	$\Delta P^a$	Beam laboratory momentum (GeV/c)	$t$ [(GeV/c) <sup>2</sup> ]	$P$	$\Delta P^a$		
2.50	-0.200	0.312	0.025	2.93	-0.413	0.229	0.022		
	-0.212	0.370	0.028		-0.450	0.221	0.025		
	-0.230	0.358	0.022		-0.487	0.182	0.030		
	-0.251	0.372	0.024		-0.526	0.164	0.038		
	-0.275	0.328	0.024		-0.580	0.176	0.037		
	-0.303	0.312	0.026		-0.626	0.176	0.040		
	-0.328	0.331	0.029		-0.683	0.204	0.043		
	-0.348	0.254	0.033		-0.728	0.283	0.048		
	-0.387	0.253	0.043		-0.798	0.321	0.052		
	-0.420	0.249	0.033		-0.843	0.450	0.059		
	-0.471	0.198	0.033		-0.805	0.432	0.055		
	-0.503	0.161	0.036		-0.954	0.620	0.056		
	-0.537	0.116	0.039		-1.0115	0.588	0.053		
	-0.582	0.137	0.047		-1.085	0.479	0.037		
	-0.628	0.050	0.056		-1.208	0.588	0.041		
	-0.667	0.119	0.061		-1.372	0.591	0.041		
	-0.712	0.065	0.065		-1.450	0.562	0.046		
	-0.755	0.127	0.077						
	-0.802	0.208	0.080						
	-0.846	0.284	0.080						
	2.75	-0.895	0.218		0.074	3.25	-0.184	0.310	0.029
		-0.931	0.221		0.067		-0.194	0.256	0.015
-0.977		0.338	0.070	-0.213	0.248		0.021		
-1.019		0.467	0.067	-0.221	0.253		0.011		
-1.066		0.549	0.070	-0.248	0.250		0.010		
				-0.268	0.233		0.020		
				-0.286	0.239		0.011		
				-0.320	0.203		0.010		
				-0.358	0.201		0.012		
				-0.392	0.163		0.012		
				-0.430	0.164		0.015		
				-0.468	0.154		0.015		
				-0.509	0.117		0.020		
				-0.538	0.119		0.034		
				-0.559	0.106		0.024		
				-0.600	0.106		0.029		
				-0.614	0.087		0.042		
				-0.666	0.115		0.031		
				-0.744	0.297		0.044		
				-0.844	0.420		0.019		
				-0.950	0.476		0.089		
				-1.001	0.553		0.025		
			-1.128	0.653	0.025				
			-1.257	0.639	0.025				
			-1.306	0.766	0.100				
			-1.394	0.682	0.028				
			-1.529	0.653	0.037				
			-1.662	0.661	0.048				
			-1.795	0.576	0.056				
2.93	-0.219	0.268	0.021	3.75	-0.220	0.268	0.021		
	-0.233	0.262	0.019		-0.230	0.229	0.019		
	-0.255	0.252	0.014		-0.259	0.252	0.011		
	-0.283	0.242	0.014		-0.293	0.222	0.011		
	-0.313	0.236	0.015		-0.337	0.206	0.012		
	-0.347	0.220	0.017						
	-0.375	0.231	0.020						

TABLE I (Continued)

Beam laboratory momentum (GeV/c)	$t$ [(GeV/c) <sup>2</sup> ]	$P$	$\Delta P^a$	Beam laboratory momentum (GeV/c)	$t$ [(GeV/c) <sup>2</sup> ]	$P$	$\Delta P^a$	
3.75	-0.376	0.217	0.013	4.40	-0.694	0.123	0.057	
	-0.422	0.166	0.015		-0.750	0.097	0.067	
	-0.468	0.164	0.017		-0.866	0.323	0.064	
	-0.519	0.117	0.019		-0.974	0.412	0.105	
	-0.568	0.146	0.023		-1.048	0.365	0.111	
	-0.619	0.069	0.026		-1.134	0.634	0.118	
	-0.676	0.082	0.031		-1.419	0.545	0.080	
	-0.735	0.122	0.038		-1.608	0.578	0.095	
	-0.782	0.199	0.045		-1.819	0.574	0.133	
	-0.854	0.263	0.056		-2.033	0.486	0.191	
	-1.269	0.460	0.046		5.15	-0.221	0.257	0.026
	-1.157	0.486	0.031			-0.278	0.189	0.025
	-1.287	0.525	0.032			-0.339	0.130	0.027
	-1.460	0.552	0.037			-0.409	0.105	0.032
	-1.633	0.578	0.043			-0.479	0.056	0.038
-1.806	0.546	0.066	-0.573	0.062		0.048		
-1.955	0.600	0.095	-0.638	-0.019		0.059		
-2.125	0.551	0.153	-0.733	0.100		0.073		
4.40	-0.141	0.148	0.111	-0.825		0.073	0.102	
	-0.169	0.164	0.036	-0.923		0.316	0.107	
	-0.203	0.198	0.026	-1.004		0.316	0.132	
	-0.244	0.204	0.021	-1.120		0.446	0.158	
	-0.293	0.166	0.020	-1.216		0.418	0.153	
	-0.343	0.177	0.022	-1.330		0.609	0.201	
	-0.392	0.179	0.022	-1.451		0.506	0.214	
	-0.446	0.090	0.026	-1.552	0.375	0.236		
	-0.502	0.104	0.032	-1.669	0.578	0.305		
	-0.562	0.067	0.037	-1.810	0.423	0.299		
	-0.628	0.085	0.044					

<sup>a</sup> Errors quoted above are statistical only. There is an additional systematic error of  $\pm 10\%$  due to uncertainty in the target polarization and an absolute error of 0.015 due to uncertainty in beam normalization.

TABLE II. Measured values of polarization in  $\pi^-p$  elastic scattering.

Beam laboratory momentum (GeV/c)	$t$ [(GeV/c) <sup>2</sup> ]	$P$	$\Delta P^a$	Beam laboratory momentum (GeV/c)	$t$ [(GeV/c) <sup>2</sup> ]	$P$	$\Delta P^a$	
2.75	-0.180	-0.227	0.046	2.75	-1.380	-0.760	0.107	
	-0.220	-0.141	0.023		-1.482	-0.771	0.119	
	-0.279	-0.097	0.025		-1.571	-0.730	0.115	
	-0.344	-0.021	0.029		-1.701	-0.595	0.142	
	-0.412	-0.015	0.036		-1.812	-0.344	0.160	
	-0.492	0.045	0.048		-1.921	-0.169	0.179	
	-0.568	0.121	0.066		-2.042	-0.273	0.175	
	-0.649	0.030	0.084		-2.136	-0.037	0.267	
	-0.739	-0.254	0.109		3.25	-0.182	-0.131	0.028
	-0.820	-0.573	0.108			-0.242	-0.209	0.026
	-0.913	-0.681	0.094			-0.304	-0.118	0.026
	-1.010	-0.884	0.095			-0.367	-0.035	0.029
	-1.100	-0.841	0.084			-0.445	-0.031	0.035
	-1.193	-0.928	0.093					
	-1.282	-0.813	0.093					

TABLE II (Continued)

Beam laboratory momentum (GeV/c)	$t$ [(GeV/c) <sup>2</sup> ]	$P$	$\Delta P^a$	Beam laboratory momentum (GeV/c)	$t$ [(GeV/c) <sup>2</sup> ]	$P$	$\Delta P^a$
3.25	-0.514	0.057	0.041	4.40	-0.249	-0.168	0.021
	-0.599	0.156	0.054		-0.281	-0.070	0.017
	-0.686	0.026	0.066		-0.314	-0.089	0.013
	-0.760	-0.085	0.084		-0.352	-0.081	0.017
	-0.866	-0.304	0.091		-0.427	-0.035	0.021
	-0.951	-0.461	0.087		-0.499	0.041	0.026
	-1.062	-0.533	0.083		-0.582	0.047	0.035
	-1.149	-0.507	0.080		-0.676	0.010	0.045
	-1.250	-0.563	0.092		-0.763	-0.114	0.058
	-1.364	-0.601	0.097		-0.863	-0.237	0.068
	-1.460	-0.636	0.112		-0.960	-0.392	0.072
	-1.562	-0.469	0.122		-1.071	-0.394	0.076
	-1.685	-0.496	0.149		-1.176	-0.387	0.071
	-1.817	-0.661	0.198		-1.287	-0.520	0.073
	-1.985	-0.687	0.292		-1.394	-0.492	0.079
	-2.120	-0.530	0.348		-1.508	-0.630	0.095
	3.75	-0.265	-0.097		0.016	-1.625	-0.463
-0.323		-0.061	0.017	-1.752	-0.447	0.174	
-0.395		-0.049	0.022	-1.873	-0.133	0.234	
-0.467		0.034	0.027	5.15	-0.249	-0.135	0.019
-0.542		0.046	0.035		-0.314	-0.069	0.021
-0.632		0.056	0.044		-0.382	-0.049	0.024
-0.721		-0.058	0.056		-0.453	0.002	0.030
-0.807		-0.234	0.069		-0.531	0.048	0.038
-0.905		-0.290	0.073		-0.617	0.052	0.051
-1.010		-0.412	0.076		-0.720	-0.017	0.072
-1.106		-0.374	0.068		-0.808	-0.093	0.092
-1.205		-0.435	0.073		-0.910	-0.222	0.099
-1.317		-0.499	0.088		-1.018	-0.393	0.107
-1.427		-0.305	0.095		-1.121	-0.511	0.115
-1.536		-0.416	0.102		-1.227	-0.591	0.124
-1.651		-0.444	0.126		-1.355	-0.489	0.152
-1.783		-0.410	0.154		-1.464	-0.776	0.200
-1.988	-0.007	0.154	-1.594		-0.384	0.243	
-2.215	-0.205	0.353	-1.723		-0.668	0.280	
4.40	-0.126	-0.102	0.043		-1.840	-0.495	0.365
	-0.172	-0.113	0.032	-1.991	-0.625	0.569	
	-0.226	-0.100	0.024				

<sup>a</sup> Errors quoted above are statistical only. There is an additional systematic error of  $\pm 10\%$ .

peak-to-background ratio at a given angle, but, in the region where it is most important, results in an absolute error of 0.015 in the value of the measured polarization. In some cases this is comparable to the statistical error and to the relative  $\pm 10\%$  error due to uncertainty in the target polarization.

Two other possible sources of systematic error were considered. The direction of target polarization was reversed by a change in the polarized proton-target magnetic field. Although the field

change was only 50 G out of 17.5 kG, the effect is amplified by the steepness of the differential cross section in the forward direction. However, a calculation showed this effect to be less than 0.5% and the correction was therefore neglected.

The other source of systematic error considered was the possibility of proton contamination of the pion beam due to spurious pion signals from the pion Čerenkov counter caused by  $\delta$  rays produced by protons. Calculations showed that this effect also was less than 0.5% and it too was neglected.

TABLE III. Measured values of polarization in backward  $\pi^+p$  elastic scattering.

Laboratory momentum (GeV/c)	$\cos\theta_{c.m.}$	$u$ [(GeV/c) <sup>2</sup> ]	$\Delta u$ [(GeV/c) <sup>2</sup> ]	$P$	
2.50	-0.744	-0.371	0.031	-0.04 ± 0.10	
	-0.771	-0.318	0.030	-0.07 ± 0.10	
	-0.796	-0.269	0.028	0.04 ± 0.13	
	-0.818	-0.224	0.026	0.30 ± 0.13	
	-0.839	-0.183	0.025	0.29 ± 0.13	
	-0.858	-0.146	0.023	0.56 ± 0.13	
	-0.876	-0.112	0.022	0.47 ± 0.14	
	-0.891	-0.081	0.020	0.54 ± 0.16	
	-0.905	-0.053	0.019	0.82 ± 0.17	
	-0.918	-0.028	0.017	1.27 ± 0.19	
	-0.931	-0.003	0.016	0.75 ± 0.19	
	-0.946	0.026	0.017	0.49 ± 0.10	
	-0.962	0.058	0.014	0.17 ± 0.07	
	-0.976	0.085	0.011	0.09 ± 0.07	
	-0.988	0.108	0.009	0.09 ± 0.05	
	-0.996	0.125	0.005	0.00 ± 0.10	
	2.75	-0.757	-0.411	0.034	-0.30 ± 0.10
		-0.782	-0.356	0.032	-0.10 ± 0.09
		-0.806	-0.304	0.030	-0.01 ± 0.10
		-0.827	-0.257	0.029	0.03 ± 0.11
-0.848		-0.212	0.027	0.55 ± 0.14	
-0.866		-0.172	0.025	0.66 ± 0.16	
-0.882		-0.136	0.023	1.21 ± 0.17	
-0.897		-0.104	0.022	0.99 ± 0.16	
-0.910		-0.075	0.020	0.79 ± 0.17	
-0.922		-0.050	0.019	0.70 ± 0.17	
-0.935		-0.021	0.017	0.66 ± 0.22	
-0.948		0.009	0.018	0.24 ± 0.08	
-0.964		0.043	0.015	0.13 ± 0.06	
-0.977		0.071	0.012	-0.02 ± 0.05	
-0.986		0.092	0.009	0.04 ± 0.04	
-0.993		0.106	0.006	0.06 ± 0.05	
2.93		-0.765	-0.440	0.036	-0.36 ± 0.10
		-0.789	-0.382	0.034	-0.05 ± 0.11
		-0.812	-0.328	0.032	-0.23 ± 0.13
		-0.833	-0.279	0.030	0.26 ± 0.11
	-0.852	-0.233	0.028	0.15 ± 0.14	
	-0.870	-0.191	0.027	0.51 ± 0.15	
	-0.886	-0.154	0.025	0.59 ± 0.17	
	-0.900	-0.120	0.023	0.76 ± 0.20	
	-0.913	-0.090	0.022	0.17 ± 0.20	
	-0.924	-0.063	0.020	0.48 ± 0.17	
	-0.937	-0.033	0.018	0.41 ± 0.11	
	-0.950	-0.002	0.019	0.21 ± 0.09	
	-0.965	0.033	0.016	0.07 ± 0.06	
	-0.977	0.062	0.013	0.12 ± 0.07	
	-0.987	0.084	0.010	0.04 ± 0.06	
	-0.994	0.102	0.007	0.10 ± 0.08	
	3.25	-0.790	-0.451	0.049	-0.76 ± 0.09
		-0.834	-0.336	0.043	-0.54 ± 0.12
		-0.870	-0.239	0.037	-0.03 ± 0.18
		-0.900	-0.160	0.032	0.29 ± 0.25
-0.924		-0.095	0.027	0.18 ± 0.22	

TABLE III (Continued)

Laboratory momentum (GeV/c)	$\cos\theta_{c.m.}$	$u$ [(GeV/c) <sup>2</sup> ]	$\Delta u$ [(GeV/c) <sup>2</sup> ]	$P$
3.25	-0.941	-0.051	0.020	0.10 ± 0.26
	-0.953	-0.019	0.020	-0.05 ± 0.11
	-0.970	0.027	0.019	-0.07 ± 0.08
	-0.985	0.067	0.013	-0.04 ± 0.06
	-0.994	0.090	0.008	0.19 ± 0.16
3.75	-0.808	-0.504	0.054	-0.81 ± 0.10
	-0.848	-0.381	0.047	-0.59 ± 0.14
	-0.881	-0.277	0.041	-0.49 ± 0.19
	-0.920	-0.156	0.047	0.23 ± 0.37
	-0.954	-0.052	0.028	-0.10 ± 0.27
	-0.973	0.008	0.021	0.10 ± 0.15
	-0.986	0.050	0.015	-0.08 ± 0.08
	-0.994	0.076	0.009	-0.08 ± 0.13

## IV. DISCUSSION AND CONCLUSIONS

If  $\pi p$  elastic scattering is regarded as taking place through particle exchange, the quantum numbers of the exchange are established by considering the  $t$ -channel pion-pion state. The allowed quantum numbers belong to two sequences:

$$I^G(J^P) = 0^+(0^+, 2^+, 4^+, \dots)$$

and

$$I^G(J^P) = 1^+(1^-, 3^-, \dots),$$

with the  $f(1260)$  and  $\rho(765)$  mesons the leading particles in each series, respectively. At small  $-t$  the Pomeron dominates in the  $I=0$  series.

In terms of the invariant amplitudes, the polarization is

$$P = -\frac{\sin\theta}{16\pi\sqrt{s}} \left[ \frac{\text{Im}(AB^*)}{\sigma} \right], \quad (1)$$

in which  $\theta$  is the center-of-momentum scattering angle,  $s$  is the total center-of-momentum energy squared,  $\sigma$  is the unpolarized differential cross section, and  $A$  and  $B$  are the invariant amplitudes for the helicity-nonflip and -flip processes, respectively.<sup>19</sup> The addition of isospin to form the  $t$ -channel dipion state leads to the following relationships between the amplitudes for  $\pi^+p$  elastic and  $\pi^-p$  charge-exchange scattering and the amplitudes for the exchange of  $I=0$  and  $I=1$  objects:

$$\pi^\pm + p \rightarrow \pi^\pm + p, \quad A_\pm = A_0 \pm A_1, \quad B_\pm = B_0 \pm B_1, \quad (2)$$

$$\pi^- + p \rightarrow \pi^0 + n, \quad A_x = -\sqrt{2} A_1, \quad B_x = -\sqrt{2} B_1. \quad (3)$$

The polarization for  $\pi^\pm p$  elastic scattering then has the form

$$P_\pm = -\frac{\sin\theta}{16\pi\sqrt{s}\sigma_\pm} \text{Im}[(A_0 B_0^* + A_1 B_1^*) \pm (A_0 B_1^* + A_1 B_0^*)] \quad (4)$$

or

$$P_\pm = -\frac{\sin\theta}{16\pi\sqrt{s}\sigma_\pm} (F_s \mp F_a). \quad (5)$$

Thus the polarization arises from two types of terms: one,  $F_s$ , contributing with the same sign to  $\pi^+$  and  $\pi^-$  scattering, the other,  $F_a$ , contributing with change of sign. When  $F_s$  is small compared to  $F_a$  the polarization is mirror-symmetric between  $\pi^+$  and  $\pi^-$  scattering provided the differential cross sections are approximately equal. Increasing the size of  $F_s$  produces a deviation from the mirror symmetry, and where  $F_s$  dominates, the polarizations are approximately equal. Note that  $F_s$  arises from interference between  $I=0$  exchanges or  $I=1$  exchanges, whereas  $F_a$  is due to interference between  $I=0$  and  $I=1$ .

The general features of the  $t$  dependence can now be described in terms of  $F_s$  and  $F_a$ . The principal apparent feature in Fig. 2 is that  $F_a$  dominates and the  $\pi^+$  and  $\pi^-$  polarizations are nearly mirror-symmetric. Both have a dip near  $t = -0.6$  (GeV/c)<sup>2</sup> where they are essentially zero (at least at momenta above 5 GeV/c) and have relatively large polarizations at large values of  $-t$ .

Even at high momenta, however, there is a noticeable departure from mirror symmetry in the region between  $t=0$  and  $t=-0.6$  where the  $\pi^-$  polarization is consistently smaller in magnitude than the  $\pi^+$ . At lower momenta, increasing asymmetry is apparent at the dip where the polarization rises toward positive values for both  $\pi^+$  and  $\pi^-$  while the difference remains zero within errors.

The points taken at largest values of  $-t$  indicate that the  $\pi^-$  polarization is rising and possibly crossing zero while there is no corresponding fall of the  $\pi^+$  data.

Since the data were collected at several (although relatively closely spaced) energies, it is possible to study the energy dependence for a fixed value of  $t$ . In Fig. 3 the polarizations at fixed  $t$  are plotted against the laboratory momentum of the beam. In order to extend the range of momentum we have supplemented the data of this experiment with data at higher and lower momenta from Refs. 6, 12, and 13. These points at fixed  $t$  were obtained by an error-weighted linear interpolation between data points. The most striking feature of these plots is the flatness of the polarization at fixed  $t$  over the momentum range covered by existing data above 3 GeV/c. Below 3 GeV/c the behavior of the polarization is complicated by resonances. Confining attention to the data above 3 GeV/c, the energy dependence may be briefly described as fol-

lows: At  $t = -0.3$  the  $\pi^+$  polarization decreases to a constant (or slowly varying) positive value while the  $\pi^-$  polarization is flat over the entire range; at  $t = -0.6$ ,  $\pi^+$  and  $\pi^-$  polarizations are nearly equal over the entire range and both high-energy levels are consistent with zero; at  $t = -0.9$ , the mirror symmetry has returned so that both  $\pi^+$  and  $\pi^-$  high-energy levels are approximately equal in magnitude and opposite in sign

One can also see qualitatively the behavior of  $F_s$  and  $F_a$  defined in Eq. (5) and how they affect  $P_{\pm}$ . As emphasized before,  $F_a$  gives the mirror symmetry and vanishes at  $-t = 0.6$ . At this  $t$  value we see only  $F_s$ . It gives a positive contribution to both  $P_+$  and  $P_-$  and decreases rapidly with increasing momentum. Thus one can understand the strong energy dependence of  $P_+$  at low  $-t$  and the fact that here  $P_-$  is almost energy-independent;  $F_s$  and  $F_a$  work together in  $P_+$  while their energy dependences almost cancel in  $P_-$ .

Where both the polarizations  $P_{\pm}$  and the differ-

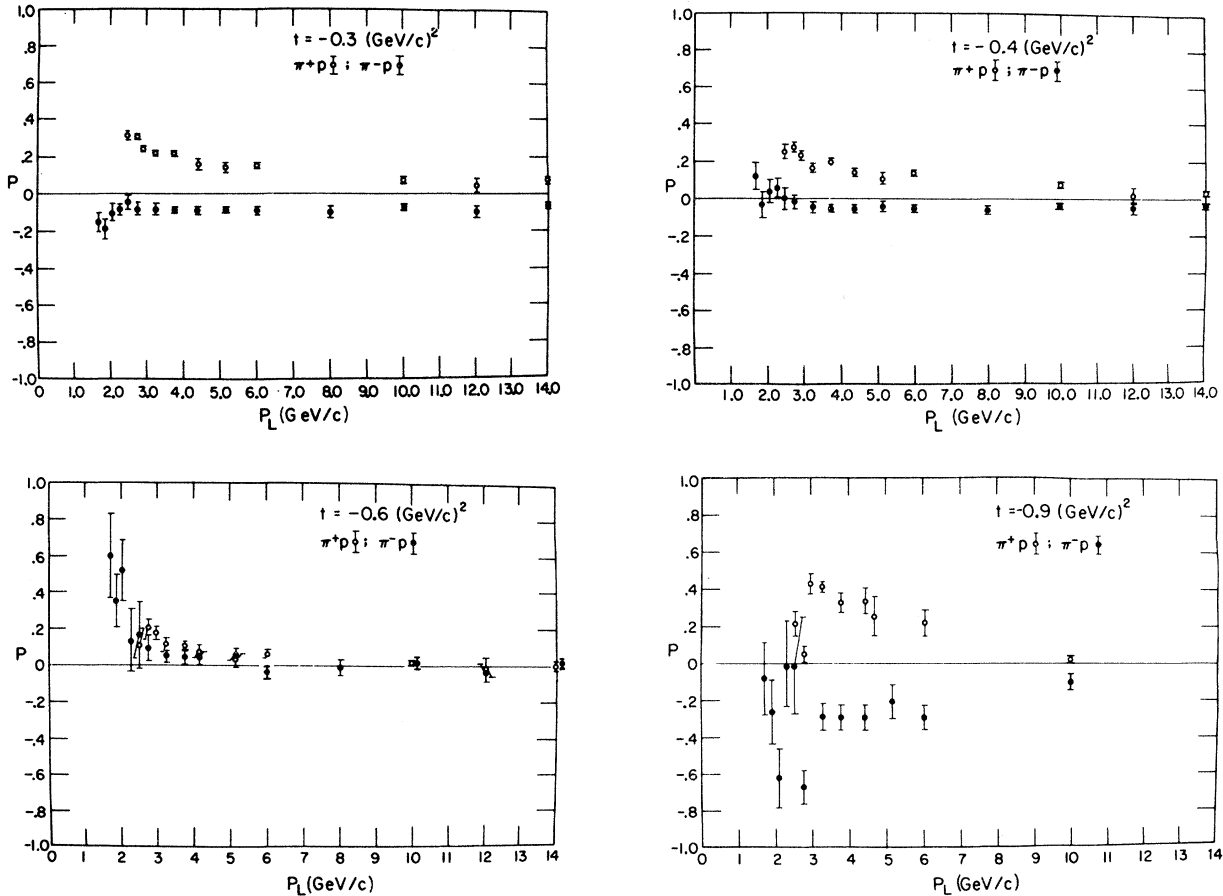


FIG. 3. Interpolated polarization in  $\pi p$  elastic scattering at fixed values of  $t$  plotted against pion laboratory momentum. Below 2.50 GeV/c the data of Ref. 6 were used; above 5.15 GeV/c the data of Refs. 12 and 13 were used; the points between 2.50 and 5.15 GeV/c are from this experiment.

ential cross sections  $\sigma_{\pm}$  for  $\pi^+$  and  $\pi^-$  scattering are available, it is possible to calculate  $F_s$  and  $F_a$  and therefore to study the amplitudes more directly.<sup>4,20</sup> In terms of the measured polarizations and differential cross sections

$$F_s = -\frac{8\pi\sqrt{s}}{\sin\theta} (P_+\sigma_+ + P_-\sigma_-) = \text{Im}(A_0B_0^* + A_1B_1^*), \quad (6)$$

$$F_a = +\frac{8\pi\sqrt{s}}{\sin\theta} (P_+\sigma_+ - P_-\sigma_-) = \text{Im}(A_0B_1^* + A_1B_0^*). \quad (7)$$

We also have

$$-\frac{8\pi\sqrt{s}}{\sin\theta} P_x\alpha_x = \text{Im}(A_1B_1^*), \quad (8)$$

where  $P_x$  and  $\alpha_x$  are the polarization and cross section in charge-exchange scattering. In order to calculate  $F_s$  and  $F_a$  it was necessary to use polarization values obtained by interpolating to regular intervals of  $t$  so that data points for both  $\pi^+$  and  $\pi^-$  were available at the same  $t$  values. The differential cross-section values were not obtained by interpolation from experimental data, but by using the 5-pole parametrization of Barger and Phillips which fits the data very well over a large

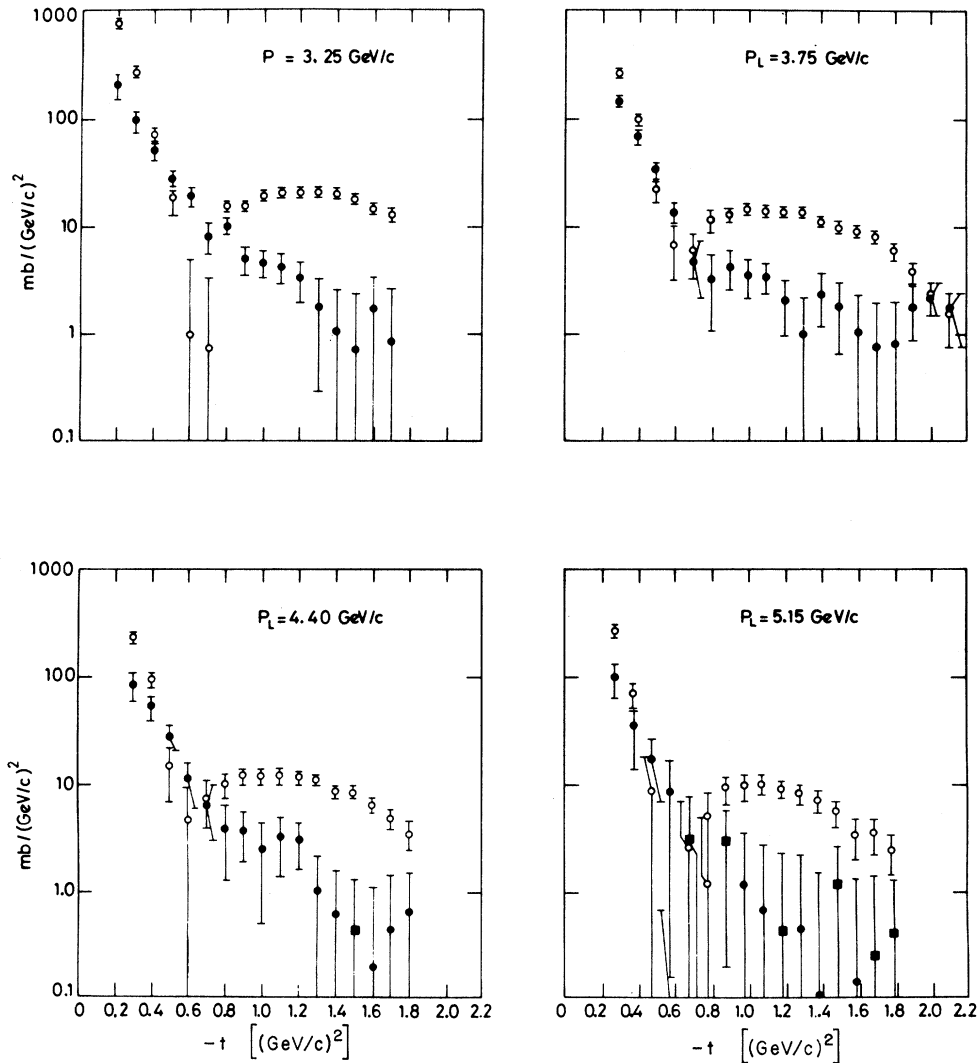


FIG. 4. Plots of  $F_a$  and  $-F_s$  (open and filled points, respectively) vs  $t$ . The values were calculated using the polarization data of this experiment and differential cross-section values obtained using the model of Ref. 16. The filled square points indicate positive values of  $F_s$ .

range of energy and momentum transfer.<sup>16</sup> Errors in the differential cross sections were neglected since they are in general much smaller than those in the polarizations.

The results are presented in Fig. 4 in which  $F_s$  and  $F_a$  are plotted against  $t$  at several momenta. In these plots, the points where  $F_s$  and  $F_a$  cross correspond closely to the points where  $P_-$  goes through zero; where  $P_-$  is positive,  $F_s$  is larger than  $F_a$ . The most important feature of these plots is simply the size of  $F_s$ , which is not so obvious for example in Fig. 2, and, contrary to a common assumption in Regge models, this term is not negligible. The prominent feature in  $F_a$  is the deep dip at  $t \approx -0.6$  (GeV/c)<sup>2</sup> unaccompanied by a corresponding dip in  $F_s$ . However, there is apparently a kink in the  $t$  dependence of  $F_s$  at about this  $t$  value.

In an earlier publication<sup>4</sup> we discussed the  $t$  dependence of  $F_s$  and  $F_a$  in terms of the expected dominant Regge poles  $P$  and  $f$  for the  $I=0$  amplitudes, and  $\rho$  for the  $I=1$  amplitudes. Within the framework of that model we were able to show that the form

$$B_1 \propto \frac{\alpha_p (1 - e^{i\pi\alpha_p})}{\sin \pi\alpha_p}, \quad \alpha_p = 0.5 + 0.9t \quad (9)$$

where  $\alpha_p$  is the  $\rho$  trajectory, explains the double zeros at  $t = -0.6$  and the approximate mirror symmetry of  $P_{\pm}$ , and thereby the general behavior of  $F_a$ . Strictly speaking, this explanation is valid beyond  $t = -0.6$  only if  $\text{Im}(A_0)$  does not change sign near  $t = -0.6$ . The energy dependence of  $d\sigma/dt$  for  $-t > 0.6$  suggests that  $d\sigma/dt$  and therefore  $\text{Im}(A_0)$  is dominated by the  $f$  in this region. Since  $\text{Im}(A_f)$  [the contribution of the  $f$  to  $\text{Im}(A_0)$ ] must have at least a single zero at  $\alpha_f = 0$ , the inference then is that it has a double zero. However,  $P$ - $f$  interference cannot then explain the behavior of  $F_s$ , which would consequently have to be zero at  $-t = 0.6$ . Note that from Eq. (6) the term  $\text{Im}(A_1 B_1^*)$  also contributes to  $F_s$  and can be evaluated from charge-exchange data. Even with the new results<sup>21</sup> on  $P_x$  which give larger values than the previous ones,<sup>22</sup>  $\text{Im}(A_1 B_1^*)$  is only about 10% of  $\text{Im}(A_0 B_0^*)$  at  $t = -0.6$  and cannot account for its large values at  $t = -0.6$ .

Barger and Phillips<sup>16</sup> proposed a solution to this dilemma by introducing two new poles, the  $f'$  and the  $\rho'$  lying one half unit of angular momentum lower than the  $f$  and  $\rho$ . In their model the  $\rho'$  accounts for the fact that  $P_x$  is nonzero, while the  $f'$ , by interfering with  $P$  and  $f$ , produces the observed  $F_s$ . The imaginary part of  $A_f$  has a double zero, as we concluded earlier, but  $F_s$  remains large at  $t = -0.6$  because of  $P$ - $f'$  interference. The  $f'$ , lying lower than the  $f$ , also gives  $F_s$  a strong energy dependence. Although this 5-pole model may seem

artificial, it offers a satisfactory parametrization of most existing experimental data, including some of the results from this experiment.<sup>23</sup> In fact it gives a reasonable fit to the amplitudes themselves over the limited range of  $t$  for which they have been determined from recent  $\pi N$  amplitude analysis.<sup>24</sup>

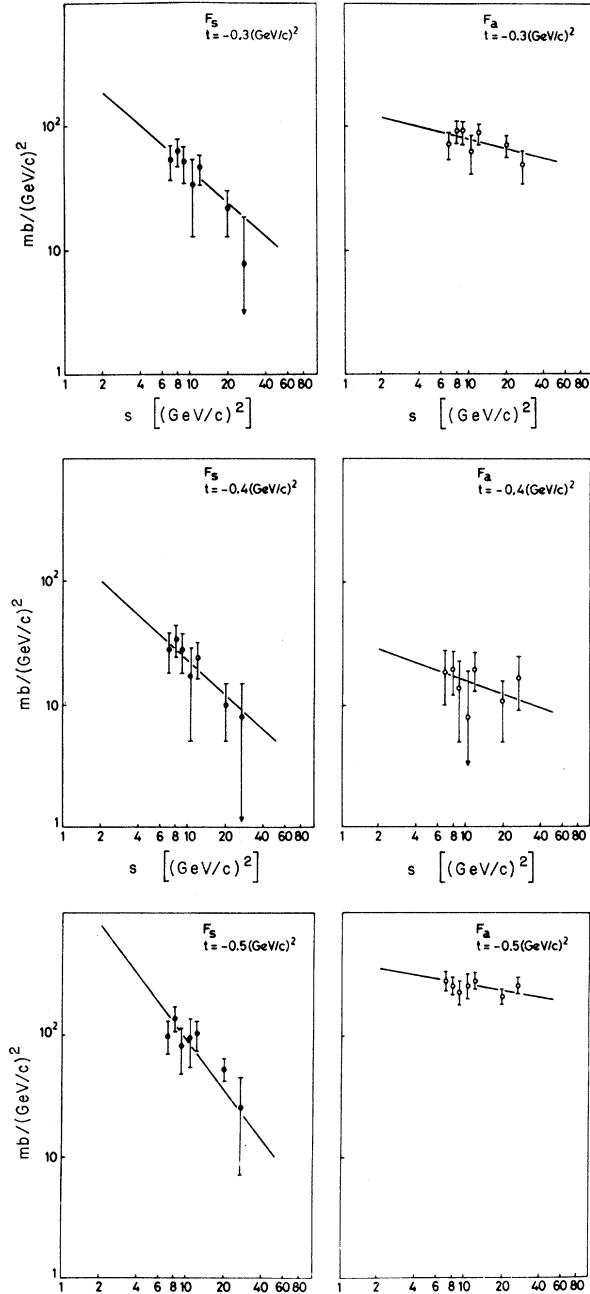


FIG. 5. Log-log plot of the symmetric and antisymmetric components  $F_a$  and  $-F_s$  (plotted as open and filled points, respectively) vs  $s$  for fixed  $t$  values of  $-0.3$ ,  $-0.4$ , and  $-0.5$  (GeV/c)<sup>2</sup>. The lines represent the results of fitting with the form  $Cs^\alpha$ .

However, the amplitude analysis has been carried out at only one momentum, 6 GeV/c, and, having determined  $F_s$  and  $F_a$ , it is interesting to look at their energy dependences in order to try to gain some insight into the behavior with energy of the amplitudes.

As an example of the energy dependence of  $F_s$  and  $F_a$  for a fixed value of  $t$ , Fig. 5 shows  $\log F_a$  and  $\log F_s$  plotted against  $\log s$  for  $-t=0.3, 0.4$ ,

and  $0.5 \text{ (GeV/c)}^2$ . Within the errors the plots are linear at all  $t$  values for both  $F_s$  and  $F_a$ . They can therefore be considered to have the form  $s^{\alpha_{\text{eff}}(t)}$ . If  $F_s$  or  $F_a$  is due to interference between the exchange of two Regge trajectories  $\alpha_1$  and  $\alpha_2$ , then  $\alpha_{\text{eff}} = \alpha_1 + \alpha_2 - 1$ . The exponent for each value of  $t$  was determined by least-squares fitting to a straight line. This analysis was done using the data of this experiment at 3.25, 3.75, 4.40, and

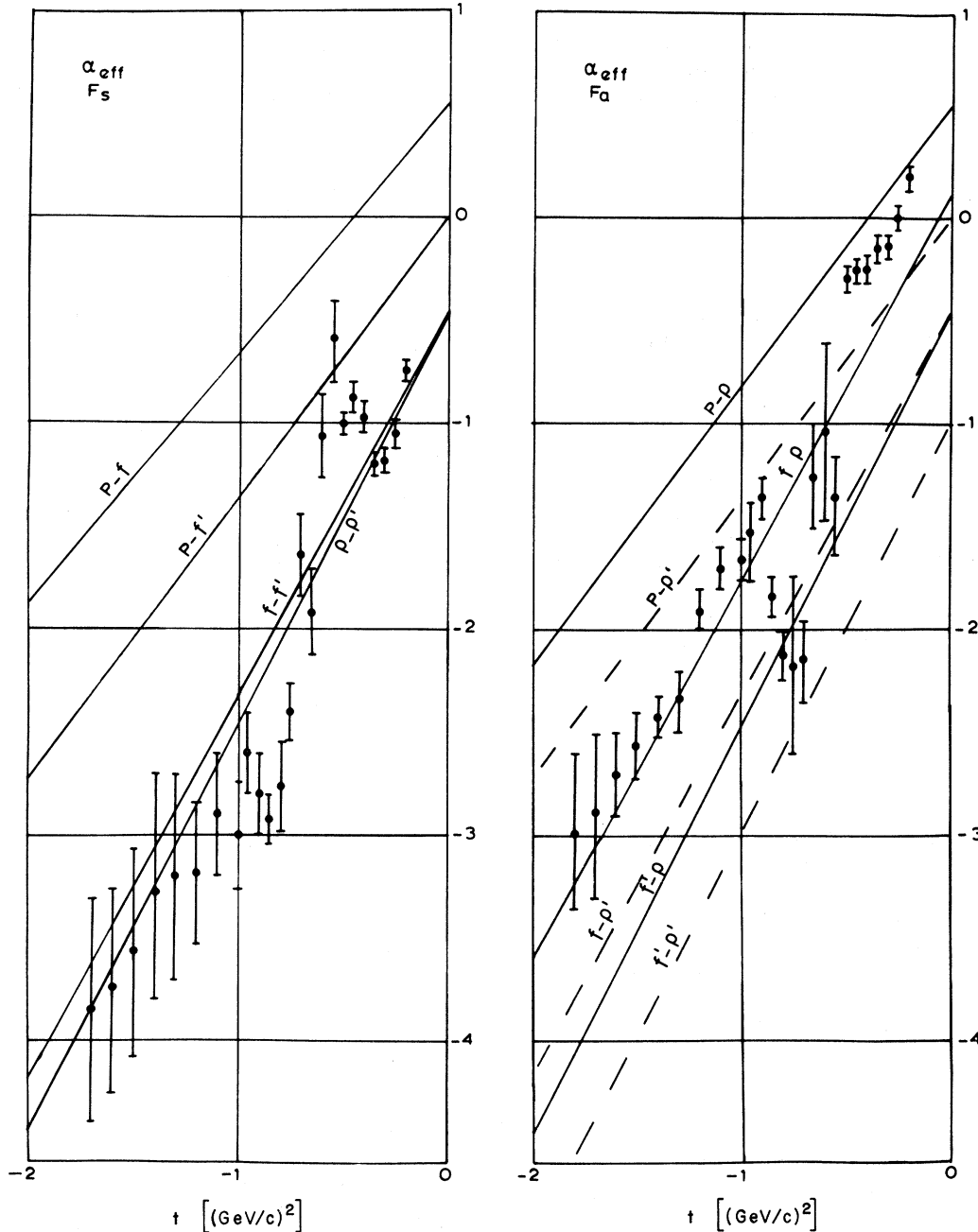


FIG. 6. Values of  $\alpha_{\text{eff}}$  obtained from the symmetric and antisymmetric terms  $F_s$  and  $F_a$  vs  $t$ . The straight lines are derived from the possible interference terms which can contribute in the model of Ref. 16.

5.15 GeV/c plus the data from Refs. 12 and 13 at 6.0, 10.0, and 14.0 GeV/c. The data below 3.25 GeV/c were excluded from this Regge trajectory analysis since, as can be seen in the plots of polarization against  $t$ , the effect of resonances is beginning to complicate the picture, causing a decrease in the goodness of fit. The results are shown in Fig. 6.

Although, considering the errors, a straight line  $\alpha_{\text{eff}} = a + bt$  is not excluded as a representation of the results of Fig. 6, there does appear to be more structure. In their fit to experimental data with the 5-pole parametrization, Barger and Phillips obtained the trajectories

$$\begin{aligned}\alpha_p &= 1 + 0.36t, \\ \alpha_\rho &= 0.55 + t, \\ \alpha_f &= 0.56 + 0.86t, \\ \alpha_{\rho'} &= \alpha_{f'} = t.\end{aligned}\tag{10}$$

Each pair of trajectories  $\alpha_i, \alpha_j$  will give a contribution to  $F_s$  or  $F_a$  of the form  $\text{Im}(A_i B_j^*) = C_{ij}(t)s^{\alpha_i + \alpha_j - 1}$ . The contribution is to  $F_s$  if  $i$  and  $j$  have the same  $I$  spin, and to  $F_a$  if they are different. In Fig. 6 we have plotted the possible lines of  $\alpha_i + \alpha_j - 1$  vs  $t$ , derived from these five trajectories, which can contribute to  $F_s$  and  $F_a$ . On neither plot do the points fall on a single line over the full range of  $t$ , and we should not expect this.

Considering first of all the plot of  $\alpha_{\text{eff}}$  for  $F_a$ , the general trend is that at small  $-t$ ,  $F_a$  is dominated by  $P$ - $\rho$  interference, but there is a transition to  $f$ - $\rho$  interference at large  $-t$ . To the extent that the apparent structure in the form of a dip at  $-t$

$\approx 0.7$  may be believed, it is consistent with the conclusion discussed earlier that  $A_f$  has a zero at  $\alpha_f = 0$  ( $t = -0.65$ ) and so at this point  $B_\rho$  must interfere with a lower-lying trajectory. Also there appears to be little influence of the  $P$  beyond  $t = -0.5$ .

Turning now to  $F_s$  we note first of all that  $\alpha_{\text{eff}}(t)$  is lower by 0.5–1 unit than it is for  $F_a$ . Also,  $P$ - $f$  interference appears to be absent, and also  $P$ - $f'$  except possibly at  $t = -0.6$ . Something similar to the  $f$ - $f'$  interference term apparently dominates  $F_s$ . To the extent that the peak at  $t = -0.6$  can be believed, it also is consistent with the vanishing of  $A_f$ . The most likely explanation for  $F_s$  is that it is mainly determined by  $\text{Im}(A_P + A_f)B_f^*$ , with the second term larger than the first except at  $t = -0.65$  where  $A_f$  vanishes. Possibly  $\rho$ - $\rho'$  interference contributes at large  $-t$  as well as  $f$ - $f'$ , but the main point is that a low-lying trajectory like the  $f'$  of Barger and Phillips is needed.

As a final conclusion we note that the results are consistent with  $s$ -channel helicity conservation<sup>25</sup> for  $P$ , and also for  $f$ , i.e.,  $B_P \cong B_f \cong 0$ . Also, the results suggest that  $B_0 \approx B_f$ , and  $B_1 \cong B_\rho$ .

#### ACKNOWLEDGMENTS

We wish to thank the many people at the Enrico Fermi Institute and the Argonne National Laboratory for their assistance and cooperation throughout the experiment. In particular we are indebted to T. Nunamaker and R. Norton for the design and construction of much of the electronics, and to A. Gonis, R. Larsen, A. Lesnick, and H. Petri for their assistance during the running and analysis of the experiment.

<sup>†</sup>Work supported by the National Science Foundation under Grant Nos. GP-6135 and GU-2175, and by the Atomic Energy Commission.

<sup>‡</sup>Paper submitted by J. A. Scheid in partial fulfillment of the requirements for the Ph.D. degree.

\*Present address: Nuclear Physics Laboratory, University of Oxford, Oxford, England.

<sup>§</sup>Present address: Rutherford High Energy Laboratory, Chilton, Didcot, Berkshire, England.

<sup>||</sup>Present address: Computer-based Education Research Laboratory, University of Illinois, Urbana, Illinois 61801.

\*\*Present address: Stanford Linear Accelerator Center, P.O. Box 4349, Stanford, California 94305.

<sup>1</sup>N. E. Booth, G. Conforto, R. J. Esterling, J. H. Parry, J. A. Scheid, D. J. Sherden, and A. Yokosawa, *Phys. Rev. Lett.* **21**, 651 (1968); *Phys. Rev. Lett.* **23**, 192 (1969).

<sup>2</sup>J. H. Parry, N. E. Booth, G. Conforto, R. J. Esterling, J. A. Scheid, D. J. Sherden, and A. Yokosawa, *Phys. Rev. D* **8**, 45 (1973).

<sup>3</sup>D. J. Sherden, N. E. Booth, G. Conforto, R. J. Esterling, J. H. Parry, J. A. Scheid, and A. Yokosawa, *Phys. Rev. Lett.*

**25**, 898 (1970).

<sup>4</sup>R. J. Esterling, N. E. Booth, G. Conforto, J. H. Parry, J. A. Scheid, D. J. Sherden, and A. Yokosawa, *Phys. Rev. Lett.* **21**, 1410 (1968).

<sup>5</sup>O. Chamberlain, M. J. Hansroul, C. H. Johnson, P. D. Grannis, L. E. Holloway, L. Valentin, P. R. Robrish, and H. M. Steiner, *Phys. Rev. Lett.* **17**, 975 (1966).

<sup>6</sup>P. J. Duke, D. P. Jones, M. A. R. Kemp, P. G. Murphy, J. J. Thresher, H. H. Atkinson, C. R. Cox, and K. S. Heard, *Phys. Rev.* **166**, 1448 (1968).

<sup>7</sup>R. E. Hill, N. E. Booth, R. J. Esterling, S. Suwa, and A. Yokosawa, *Phys. Rev. D* **1**, 729 (1970).

<sup>8</sup>M. Borghini, G. Coignet, L. Dick, K. Kuroda, L. di Lella, P. C. Macq, A. Michalowicz, and J. C. Olivier, *Phys. Lett.* **24B**, 77 (1966).

<sup>9</sup>M. Borghini, L. Dick, L. di Lella, A. Navarro, J. C. Olivier, K. Reibel, G. Coignet, D. Cronenberger, G. Grégoire, K. Kuroda, A. Michalowicz, M. Poulet, D. Sillou, C. Bellettini, P. L. Braccini, T. del Prete, L. Foa, G. Sanguinetti, and M. Valdata, *Phys. Lett.* **31B**, 405 (1970).

<sup>10</sup>M. Borghini, L. Dick, J. C. Olivier, H. Aoi, D. Cronenberger,

- G. Grégoire, Z. Janout, K. Kuroda, A. Michalowicz, M. Poulet, D. Sillou, G. Bellettini, P. L. Braccini, T. del Prete, L. Foa, P. Laurelli, G. Sanguinetti, and M. Valdata, *Phys. Lett.* **36B**, 493 (1971).
- <sup>11</sup>M. G. Albrow, S. Andersson/Almehed, B. Bošnjaković, C. Daum, F. C. Erné, J. P. Lagnaux, J. C. Sens, and F. Udo, *Nucl. Phys.* **B25**, 9 (1970).
- <sup>12</sup>M. G. Albrow, S. Andersson/Almehed, B. Bošnjaković, C. Daum, F. C. Erné, Y. Kimura, J. P. Lagnaux, J. C. Sens, and F. Udo, *Nucl. Phys.* **B37**, 594 (1972).
- <sup>13</sup>G. Bureson, D. Hill, S. Kato, P. F. M. Koehler, T. B. Novey, A. Yokosawa, D. Eartly, K. Pretzl, B. Bar. ut, A. Laasanen, and P. Steinberg, *Phys. Rev. Lett.* **26**, 338 (1971).
- <sup>14</sup>A. Citron, W. Galbraith, T. F. Kycia, B. A. Leontić, R. H. Phillips, A. Rousset, and P. H. Sharp, *Phys. Rev.* **144**, 1101 (1966); A. A. Carter *et al.*, *Phys. Rev.* **168**, 1457 (1968).
- <sup>15</sup>R. J. N. Phillips and W. Rarita, *Phys. Rev.* **139**, B1336 (1965); C. B. Chiu, R. J. N. Phillips and W. Rarita, *Phys. Rev.* **153**, 1485 (1967); C. B. Chiu, S. Chu and L. Wang, *Phys. Rev.* **161**, 1563 (1967); W. Rarita, R. J. Riddell, C. B. Chiu and R. J. N. Phillips, *Phys. Rev.* **165**, 1615 (1968); V. Barger and R. J. N. Phillips, *Phys. Rev. Lett.* **20**, 546 (1968); *Phys. Rev. Lett.* **22**, 116 (1969); *Phys. Lett.* **29B**, 503 (1969); A. Beretvas and N. E. Booth, *Phys. Rev. Lett.* **22**, 113 (1969).
- <sup>16</sup>V. Barger and R. J. N. Phillips, *Phys. Rev.* **187**, 2210 (1969).
- <sup>17</sup>J. A. Scheid, doctoral dissertation, Department of Physics, University of Chicago (unpublished).
- <sup>18</sup>The sign of the target polarization is defined as positive when parallel to the vector  $\vec{k}_i \times \vec{k}_f$ , where  $\vec{k}_i$  and  $\vec{k}_f$  are the initial and final momenta of the pion.
- <sup>19</sup>V. Singh, *Phys. Rev.* **129**, 1889 (1963).
- <sup>20</sup>N. E. Booth, Rutherford Laboratory Report No. RPP/H/58, 1969 (unpublished).
- <sup>21</sup>O. Guisan, in *Proceedings of the Second International Conference on Polarized Targets*, edited by G. Shapiro (Univ. of Calif. Press, Berkeley, Calif., 1971), p. 187; more recent results from Argonne however do not indicate such large values of  $P_x$  [D. Hill *et al.*, *Phys. Rev. Lett.* **28**, 239 (1973)].
- <sup>22</sup>P. Bonamy *et al.*, *Nucl. Phys.* **B16**, 335 (1970); D. Drobnis *et al.*, *Phys. Rev. Lett.* **20**, 274 (1968).
- <sup>23</sup>G. Conforto, in *High Energy Collisions*, edited by C. N. Yang *et al.* (Gordon and Breach, New York, 1969) p. 51.
- <sup>24</sup>F. Halzen and C. Michael, *Phys. Lett.* **36B**, 367 (1971); R. L. Kelly, *Phys. Lett.* **39B**, 635 (1972).
- <sup>25</sup>V. Barger and F. Halzen, *Phys. Rev. Lett.* **30**, 194 (1972).

### Total and Partial $\gamma p$ Cross Sections at 9.3 GeV\*

H. H. Bingham, W. B. Fretter, W. J. Podolsky,† M. S. Rabin,‡ A. H. Rosenfeld, and G. Smadja§  
*University of California and Lawrence Berkeley Laboratory, Berkeley, California 94720*

J. Ballam, G. B. Chadwick, Y. Eisenberg,|| R. Gearhart, E. Kogan,|| K. C. Moffeit, J. J. Murray,  
 P. Seyboth,\*\* C. K. Sinclair, I. O. Skillicorn,†† H. Spitzer,‡‡ and G. Wolf§§  
*Stanford Linear Accelerator Center, Stanford University, Stanford, California 94305*

(Received 12 March 1973)

We report  $\gamma p$  total, topological, and channel cross sections at 9.3 GeV from a bubble-chamber experiment using a nearly monoenergetic photon beam.

#### I. INTRODUCTION

In this paper we report photoproduction cross sections obtained by exposing the SLAC-LBL 82-in. hydrogen bubble chamber to the 9.3-GeV SLAC backscattered laser beam. The experimental procedures are similar to those of our previous experiments at 2.8 and 4.7 GeV.<sup>1</sup> The photon beam has an energy spread of 6.4% [full width at half maximum (FWHM)].

We obtain the total hadronic  $\gamma p$  cross section, topological cross sections for charged multiplicities of 1 to 9, and channel cross sections for the following channels:

$$\left. \begin{aligned} \gamma p \rightarrow p + m\pi^+ + m\pi^- \\ \gamma p \rightarrow p + m\pi^+ + m\pi^- + \pi^0 \\ \gamma p \rightarrow n + (m+1)\pi^+ + m\pi^- \end{aligned} \right\} m = 1, 2, 3, 4$$

$$\gamma p \rightarrow p + K^+ + K^- + l\pi^+ + l\pi^-, \quad l = 0, 1, 2$$

$$\gamma p \rightarrow 2p + \bar{p}.$$

In Sec. II we describe the beam and event analysis. In Sec. III the procedures for obtaining cross sections are described. Results are reported and discussed in Sec. IV.

#### II. EXPERIMENTAL PROCEDURE

##### A. Photon Beam

The beam used in this experiment was similar to that used in our lower-energy experiment and has been described in detail in Refs. 2 and 3. To obtain backscattered photons with energies  $> 6.5$  GeV at present SLAC electron beam energies, the linearly polarized red light from a Q-switched ruby laser had to be frequency doubled. We used a KDP (potassium dihydrogen phosphate) or ADP